CrystEngComm

Accepted Manuscript

ROYAL SOCIETY OF CHEMISTRY

rsc.li/crystengcomm

CrystEngComm

COMMUNICATION

Self-assembled ^{nat}LiCl-$CeCl_3$ directionally solidified eutectics for thermal neutron detection

Received 00th January 20xx,
Accepted 00th January 20xx

DOI: 10.1039/x0xx00000x

www.rsc.org/

Shuangliang Cheng,[a] Rachel E. Hunneke,[b] Mengkun Tian,[c] Eric Lukosi,[b] Mariya Zhuravleva,[d,e] Charles L. Melcher,[b,d,e] Yuntao Wu [a,*]

The novel ^{nat}LiCl-$CeCl_3$ eutectic scintillators for thermal neutron detection were synthesized by using the vertical Bridgman method. The eutectic molar ratio of LiCl and $CeCl_3$ is 0.75/0.25. The effects of solidification speed on the microstructure, optical properties, and scintillation properties under γ and neutron irradiation were studied. The grown ^{nat}LiCl-$CeCl_3$ eutectics have a lamellar structure. Excited by X-ray, the scintillation emission of the ^{nat}LiCl-$CeCl_3$ eutectics peaks at 365 nm , which relates to Ce^{3+} 5d-4f emission, and a broad and weak emission appears at 526 nm. The scintillation decay time of ^{nat}LiCl-$CeCl_3$ eutectics under γ irradiation is about 20 ns. The energy spectra under Pu/Be source irradiation indicates that the synthesized ^{nat}LiCl-$CeCl_3$ is capable of detecting thermal neutron.

Introduction

Eutectic materials are mixtures of two or more solid phases solidified simultaneously from melts corresponding to eutectic compositions. In a eutectic consisting of two different phases, one solid phase with less molar ratio is generally surrounded by the matrix phase. Thus, the typical lamellar and cylindrical structures are formed with a periodic arrangement of two phases. The solidification speed (v) and the interphase spacing (λ) of eutectics follow the Hunt-Jackson law, namely $v\lambda^2$ =constant.[1] The correlation between microstructure and solidification speed provides an effective mean of designing self-assembled eutectic materials with unique physical properties for structural and functional applications.[2] Up to now, eutectic materials were synthesized by using the Czochralski,[3] the micro-pulling down,[4, 5] and the Bridgman methods.[6-9]

Scintillation materials, which can transform high-energy photons or particles into visible or ultraviolet lights have played an essential role in the field of radiation detection, such as medical imaging, homeland security, high-energy physics, and industrial inspection. Self-assembled eutectics with tunable microstructures were recently proposed to be used as scintillation materials for next-generation X-ray and neutron imaging, which require both high spatial resolution and high detection efficiency. On one hand, halide and oxide eutectics with ordered microstructure, such as CsI-NaCl:Tl^+ and $GdAlO_3$-Al_2O_3:Ce^{3+},[3, 5, 10, 11] were developed for X-ray imaging which have remarkable optical guide performance due to the total reflection of luminescent light occurring in the fiber or matrix phase depending on their refractive indices. On the other hand, novel eutectic scintillators have been utilized for neutron detection because of the deficit of ^{3}He gas.[12] ^{6}Li-containing scintillators are promising alternatives to ^{3}He gas proportional counters due to the high Q-value of 4.8 MeV of ^{6}Li(n,α)^{3}H reaction, including Li-glass,[13] LiF/ZnS ceramics,[14] lithium indium diselenide,[15,16] Cs_2LiYCl_6:Ce^{3+},[17] $LiCaAlF_6$:Eu^{2+},[18] and LiF:Eu^{2+} crystals.[19] In the past few years, most reported eutectic neutron scintillators were fluoride-based eutectics involving ^{6}Li, such as LiF-SrF_2:Ce^{3+},[8] LiF-SrF_2:Eu^{2+},[7] LiF-$LiYF_4$,[4] and LiF-CaF_2:Eu^{2+}.[6]

In 2015, we developed the first chloride-based LiCl-$BaCl_2$:Eu^{2+} eutectic for neutron detection, which has a comparable light yield with that of commercial lithium glass.[20] The aim of this work is to develop another chloride eutectic scintillator, 75%LiCl-25%$CeCl_3$,[21] for the detection of thermal neutrons and potentially fast neutrons because of the presence of chlorine. The $CeCl_3$ phase, acting as a spectral transformer, can emit scintillation light peaking at 365 nm under ionizing irradiation and achieve a high light yield of 28,000 photons/MeV.[22] Because the refractive index of $CeCl_3$ (2.2 at 365 nm) is higher than that of $LiCl_3$ (1.67 at 365 nm),[23,24] most of the produced light is expected to propagate in the CeCl3 phase through total internal reflection. The LiCl-$CeCl_3$ eutectics were grown by the Bridgman method. To understand the effects of solidification speed on the microstructure, optical and

[a] Artificial Crystal Research Center, Shanghai Institute of Ceramics, Chinese Academy of Sciences, Shanghai 201899, China.
[b] Nuclear Engineering, University of Tennessee, Knoxville, TN 37996, USA.
[c] Department of Chemical & Biomolecular Engineering, University of Tennessee, Knoxville, TN 37996, USA.
[d] Scintillation Materials Research Center, University of Tennessee, Knoxville, TN 37996, USA.
[e] Department of Materials Science and Engineering, University of Tennessee, Knoxville, TN 37996, USA.

scintillation properties of LiCl-$CeCl_3$ eutectics, scanning electron microscopy, energy-dispersive spectroscopy, photoluminescence excitation and emission, X-ray induced radioluminescence, and Pu/Be induced pulse height spectra were used.

Experimental

Preparation of eutectics

Anhydrous, high-purity beads of (99.99%) $CeCl_3$ and LiCl (Sigma-Aldrich) were used as starting materials. The compositions were mixed according to the stoichiometry of $CeCl_3$-LiCl. The mixtures were then loaded into a quartz ampoule. The ampoule was evacuated to 10^{-6} mbar and heated to 200 °C and kept there for 10 h to remove residual water and oxygen impurities. After baking, the ampoule was sealed and transferred to the Bridgman growth furnace. It passed through a temperature gradient of about 40°C/cm at a pulling rate of 2 and 8 mm/h. Finally, the furnace was cooled to room temperature at 20 °C/h. The diameter of the ingot is 7 mm.

Microstructure and composition analysis

Scanning electron microscopy tests were performed in a Zeiss-EVO MA15 SEM machine working at 20 kV using a secondary electron detector. This machine is equipped with an Energy-dispersive X-ray spectroscopy (EDS) detector. EDS maps were acquired at micron-size scale. The elemental analyses of the EDS maps, and quantifications were performed by the Bruker-ESPRIT software.

Optical property measurements

Photoluminescence emission (PL) and excitation (PLE) spectra were obtained with a HORIBA Jobin Yvon Fluorolog-3 spectrofluorometer. The excitation light went through an excitation monochromator with a 1 nm bandpass to ensure monochromaticity. Similarly, the emission monochromator was set at a 1 nm bandpass to select emission light of a specific wavelength. In the case of emission and excitation spectra, a 450 W continuous xenon lamp was used as the excitation source. Photoluminescence decay was measured on the same spectrofluorometer using a time-correlated-single-photon counting module. HORIBA Jobin Yvon NanoLEDs (pulsed light-emitting diodes) were used as the excitation source. The duration of the light pulse was shorter than 2 ns and therefore was not deconvoluted from the much longer decay profiles.

Scintillation property measurements

The scintillation decay time was measured using a time-correlated single-photon counting setup under a ^{137}Cs gamma-ray source excitation. An X-ray tube operated at 35 kV and 0.1 mA was used as the excitation source for X-ray excited radioluminescence (RL) measurements.

Thermal neutron measurements

A Pu/Be neutron source located in the center of a 25×45×30 in^3 polyethylene moderator was used for thermal neutron response measurements. Each sample was coupled to a photomultiplier with optical grease. The PMT and scintillator were covered with tin foil and electrical tape to prevent light pollution. The pulse processing chain for the measurement consisted of a H6533 Hamamatsu photomultiplier tube assembly (PMT), CR-113 Cremat preamplifier, ORTEC 572A amplifier with a 6 ms shaping time, and ASPEC927A MCA.

Results and discussion

The LiCl-$CeCl_3$ eutectics were grown with two different pulling rates of 2 and 8 mm/hr. The as-grown ingots are shown in Fig. 1(a). The 1 mm thick slabs shown in Fig. 1(b) were cut perpendicular to the growth direction. The SEM images of the cross-sections of the LiCl-$CeCl_3$ slabs are shown in Fig. 2(a) and (c). Both eutectics show lamellar-like structure. The black and gray colored regions are associated with the LiCl and $CeCl_3$ phases, respectively. As the increase of pulling rate from 2 to 8 mm/hr, the phase thickness of LiCl and $CeCl_3$ became smaller from roughly 10 to 5 mm. The phase thickness might be critical to the ionizing energy deposition and detection spatial resolution. The variation of phase thickness with pulling rate fits the Hunt-Jackson law well. The energy-dispersive spectroscopy (EDS) images (Fig. 2(b) and (d)) shows the distribution of Ce and Cl elements, confirming the separation between $CeCl_3$ phases and LiCl phases.

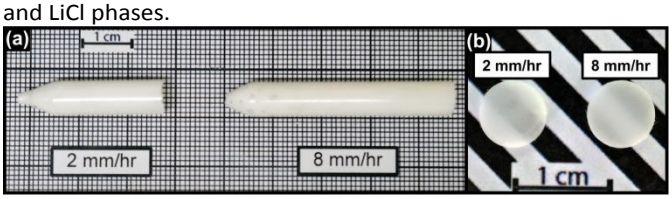

Figure 1. (a) As-grown ingots of LiCl-$CeCl_3$ eutectics grown with speeds of 2 mm/hr and 8 mm/hr, and (b) Φ7mm ×1 mm slabs.

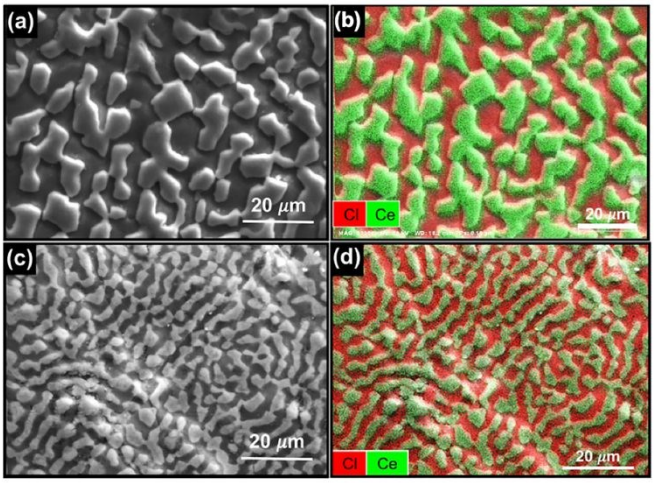

Figure 2. SEM images of transaxial cross-sections of LiCl-$CeCl_3$ slabs grown with different pulsing rates: (a) 2 mm/hr and (c) 8mm/hr, and EDS images of the same samples: (b) 2 mm/hr and (d) 8 mm/hr.

The PL excitation and emission spectra of the LiCl-$CeCl_3$ eutectic samples are shown in Fig. 3(a). As shown in emission spectra, the 340 and 365 nm emission peaks upon 265 nm

excitation are ascribed to the Ce^{3+} 5d-4f emissions. Under 310 nm excitation, the emission peaks are still at the same wavelengths but with lower intensity. In excitation spectra, when monitoring 340 and 365 nm emissions, two broad excitation bands peaking at 265 and 310 nm are observed. The PL decay profiles of LiCl-$CeCl_3$ eutectics monitoring λ_{ex}=265 nm and λ_{em}=365 nm are presented in Fig. 3(b). Both decay profiles can be well fit by a single exponential function. The decay time of the sample grown with a pulling rate of 2 mm/hr is 19.4 ns, slightly longer than the 17.7 ns of the 8 mm/hr sample.

The X-ray excited RL spectra are plotted in Fig. 3(c). An intense emission peak appears at 365 nm in both samples related to Ce^{3+} 5d-4f emission, which is consistent with the PL results. For $CeCl_3$ scintillators, its emission peak was reported to be at 360 nm when excited by a 20 keV X-ray.[22] The weak emission peak at 526 nm might be related to defect emission, such as oxygen impurities. Scintillation decay profiles under ^{137}Cs irradiation are shown in Fig. 3(d). The scintillation decay constant is 20.0 ns for the 2 mm/hr sample and 18.0 ns for the 8 mm/hr sample. Less than 1 ns difference between scintillation and PL decay constants suggests an efficient energy transfer from host to activators.

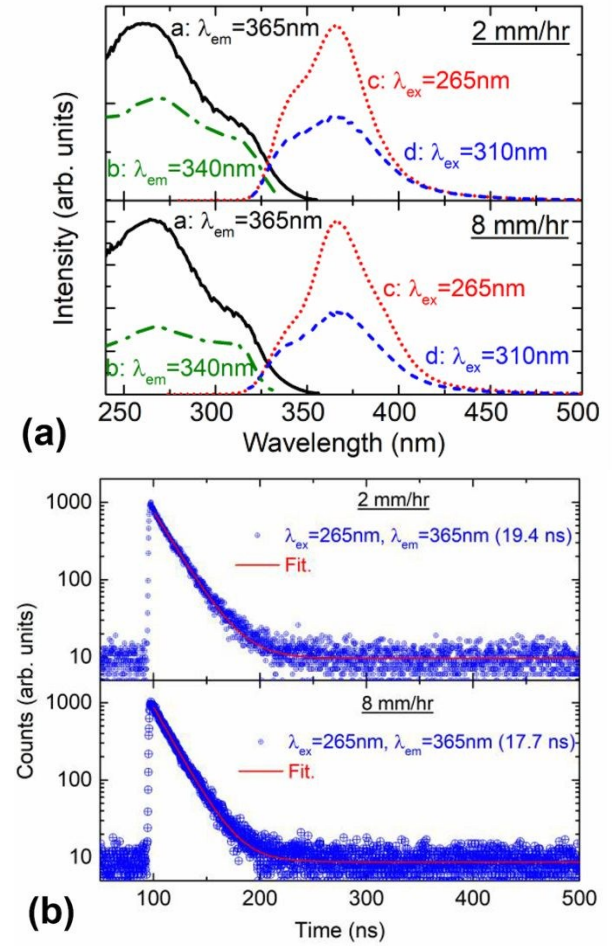

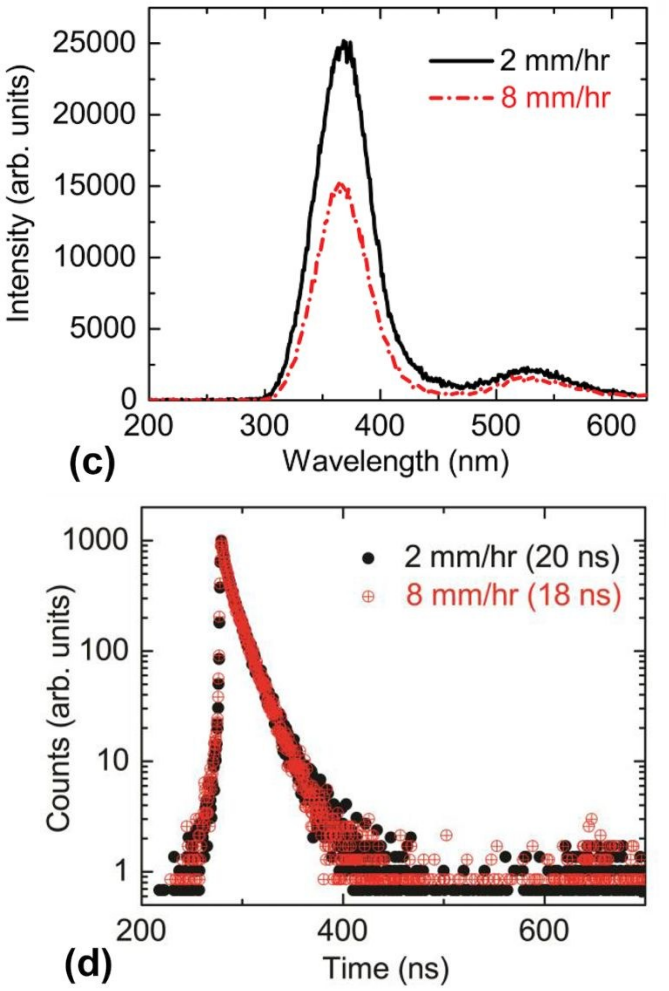

Figure 3. (a) PL and PLE spectra, (b) PL decay profile under 265 nm excitation (b), (c) X-ray excited RL spectra (c), and (d) scintillation decay profiles under ^{137}Cs irradiation of LiCl-$CeCl_3$ eutectics grown with pulling rates of 2 mm/hr and 8 mm/hr.

Fig. 4 presents pulse height spectra of the LiCl-$CeCl_3$ eutectic scintillators recorded under a Pu/Be source irradiation. A thermal neutron response above background is observed in both samples. Using SRIM[25], the calculated range of the 2.73 MeV ^{3}H particle in LiCl (ρ = 2.07 g/cm^3) and $CeCl_3$ (ρ = 3.97 g/cm^3) is 49.8 μm and 38.8 μm, respectively. For the 2.05 MeV ^{4}He particle, the respective ranges are 8.41 μm and 6.55 μm. This gives a combined range of the secondary charged particles from the ^{6}Li neutron absorption in LiCl and $CeCl_3$ of 58.21 μm and 45.35 μm, respectively. Referring to Figure 2, we can infer that the secondary charged particles may deposit its energy in only a few adjacent $CeCl_3$ regions in the sample grown at 2 mm/hr, pending the angle of emission with respect to the growth direction. For the sample grown at 8 mm/hr, the secondary charged particles more even distribute their energy loss across multiple LiCl and $CeCl_3$ regions. While the structures observed in Fig. 2 does not readily allow a full transport simulation of the secondary charged particles and the relative energy deposition in each material region, it seems reasonable to assume that the fractional energy loss in each region is roughly equal for both samples. However, the lamellar structure of the sample grown at 8 mm/hr appears more uniform, such that its light transport

efficiency to the PMT may be higher than the sample grown at 2 mm/hr. This agrees with the slightly higher mean pulse amplitude from thermal neutron exposure observed for the 8 mm/hr sample in Fig. 4. Still, the pulse amplitude observed in both samples is small given the 4.78 MeV of energy released. The first obvious reason is that more work must be conducted to optimize the growth process to produce a very well-defined, columnar lamella structure that maximizes the light transport efficiency to the PMT. Second, it has been experimentally shown that the pulse height deficit between alpha particles and betas in pure $CeCl_3$ scintillators is approximately 0.3,[26] and noting that a significant fraction of energy is lost outside of the $CeCl_3$ region explains the low pulse height amplitude. Advantageously, pulse shape discrimination is possible with $CeCl_3$, and if contamination in the growth from the actinide decay chains can be minimized, then effective thermal neutron counting may be possible. Finally, if future investigations find that pulse shape discrimination between ^1H and ^3H is possible, then the potential to count both thermal (^6Li reaction) and fast (^{35}Cl reaction[27]) neutrons while discriminating gamma background exists.

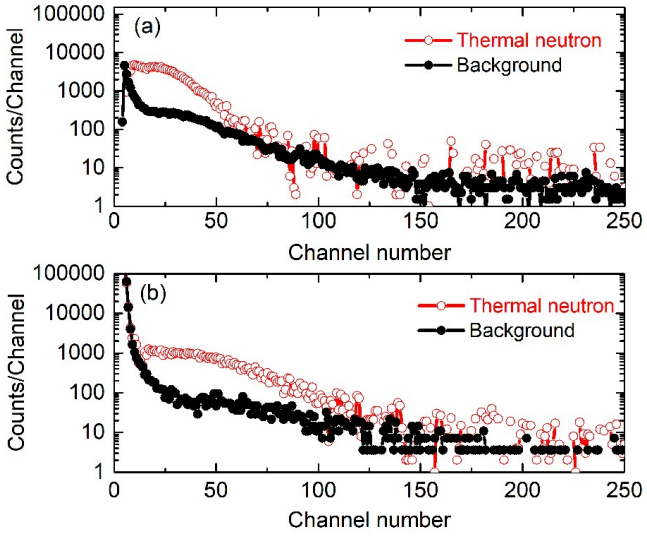

Figure 4. Cd-covered corrected spectra collected for the LiCl-$CeCl_3$ eutectic scintillators under a Pu/Be neutron source irradiation: (a) a sample grown with a pulling rate of 2 mm/hr, (b) a sample grown with a pulling rate of 8 mm/hr.

Conclusions

A new ^{nat}LiCl-$CeCl_3$ eutectic was successfully prepared by the Bridgman method for the thermal neutron detection application for the first time. The LiCl and $CeCl_3$ phases were well separated in the as-synthesized eutectics with a lamellar structure. With the increase of the pulling rate from 2 to 8 mm/hr, the phase thickness decreased from about 10 to 5 μm. The scintillation emission peak at 365 nm originated from Ce^{3+} of 5d-4f de-excitation under X-ray irradiation. There is an efficient energy transfer from $CeCl_3$ host lattice to Ce^{3+} centers. It was proven that, even using the naturally enriched lithium as starting materials, the ^{nat}LiCl-$CeCl_3$ eutectics were capable of detecting thermal neutrons. To further enhance the neutron detection efficiency and energy resolution, we will consider to use isotopically enriched lithium as starting materials, and also optimize the temperature gradient and pulling rate.

Acknowledgements

This work was supported by the National Natural Science Foundation of China (grant no. 11975303), and Youth Innovation Promotion Association funded by Chinese Academy of Sciences.

References

1 K. A. Jackson and J. D. Hunt, *Trans. Metall. Soc. AIME*, 1966, **236**, 1129-1142.
2 A. Yoshikawa, K. Kamada, S. Kurosawa, Y. Yokota, A. Yamaji, V. I. Chani, Y. Ohashi and M. Yoshino, *J. Cryst. Growth*, 2018, **498**, 170-178.
3 N. Yasui, T. Kobayashi, Y. Ohashi and T. Den, *J. Cryst. Growth*, 2014, **399**, 7-12.
4 K. Nishimoto, Y. Yokota, S. Kurosawa, Y. Fujimoto, N. Kawaguchi, K. Fukuda and A. Yoshikawa, *J. Eur. Ceram. Soc.*, 2014, **34**, 2117-2121.
5 Y. Ohashi, N. Yasui, Y. Yokota, A. Yoshikawa and T. Den, *Appl. Phys. Lett.*, 2013, **102**.
6 N. Kawaguchi, K. Fukuda, T. Yanagida, Y. Fujimoto, Y. Yokota, T. Suyama, K. Watanabe, A. Yamazaki and A. Yoshikawa, *Nucl. Instrum. Methods Phys. Res., Sect. A*, 2011, **652**, 209-211.
7 T. Yanagida, K. Fukuda, Y. Fujimoto, N. Kawaguchi, S. Kurosawa, A. Yamazaki, K. Watanabe, Y. Futami, Y. Yokota, J. Pejchal, A. Yoshikawa, A. Uritani and T. Iguchi, *Opt. Mater.*, 2012, **34**, 868-871.
8 T. Yanagida, Y. Fujimoto, K. Fukuda, N. Kawaguchi, K. Watanabe, A. Yamazaki, A. Uritani and V. Chani, *Opt. Mater.*, 2013, **35**, 1449-1454.
9 T. Yanagida, N. Kawaguchi, Y. Fujimoto, K. Fukuda, K. Watanabe, A. Yamazaki and A. Uritani, *J. Lumin.*, 2013, **144**, 212-216.
10 N. Yasui, Y. Ohashi, T. Kobayashi and T. Den, *Adv. Mater.*, 2012, **24**, 5464-5469.
11 T. Den, T. Saito, R. Horie, Y. Ohashi and N. Yasui, *IEEE Trans. Nucl. Sci.*, 2013, **60**, 16-19.
12 R. C. Runkle, A. Bernstein and P. E. Vanier, *J. Appl. Phys.*, 2010, **108**, 111101.
13 C. W. E. Van Eijk, *IEEE Trans. Nucl. Sci.*, 2012, **59**, 2242-2247.
14 H. Iikura, N. Tsutsui, T. Nakamura, M. Katagiri, M. Kureta, J. Kubo and M. Matsubayashi, *Nucl. Instrum. Methods Phys. Res., Sect. A*, 2011, **651**, 100-104.
15 E. Lukosi, E. Herrera, D. Hamm, K.-M. Lee, B. Wiggins, P. Trtik, D. Penumadu, S. Young, L. Santodonato, H. Bilheux, A. Burger, L. Matei and A. C. Stowe, *Nucl. Instrum. Methods Phys. Res., Sect. A*, 2016, **830**, 140-149.
16 B. Wiggins, M. Groza, E. Tupitsyn, E. Lukosi, K. Stassun, A. Burger and A. Stowe, *Nucl. Instrum. Methods Phys. Res., Sect. A*, 2015, **801**, 73-77.
17 C. M. Combes, P. Dorenbos, C. W. E. van Eijk, K. W. Kramer and H. U. Gudel, *J. Lumin.*, 1999, **82**, 299-305.
18 D. Totsuka, T. Yanagida, K. Fukuda, N. Kawaguchi, Y. Fujimoto, J. Pejchal, Y. Yokota and A. Yoshikawa, *Nucl. Instrum. Methods Phys. Res., Sect. A*, 2011, **659**, 399-402.

19 H. Yang, N. Menaa, F. Bronson, M. Kastner, R. Venkataraman and W. F. Mueller, *Nucl. Instrum. Methods Phys. Res., Sect. A*, 2011, **652**, 364-369.
20 Y. Wu, E. D. Lukosi, M. Zhuravleva, A. C. Lindsey and C. L. Melcher, *Nucl. Instrum. Methods Phys. Res., Sect. A*, 2015, **797**, 319-323.
21 C. Liang, Z. Chaogui, Y. Yupu, *J. Chin. Rare Earth Soc.* (China) 1990, **8**, 92-93.
22 S. E. Derenzo, W. W. Moses, J. L. Cahoon, T. A. DeVol and L. Boatner, present in part at the Conference Record of the 1991 IEEE Nuclear Science Symposium and Medical Imaging Conference, Santa Fe, NM, USA, Nov 2-9,1991.
23 C. Li, B. Wang, R. Wang and H. Wang, *Solid State Commun.*, 2007, **144**, 220-224.
24 H. H. Li, *J. Phys. Chem. Ref. Data*, 1976, **5**, 329-528.
25 J. F. Ziegler, M. D. Ziegler and J. P. Biersack, *Nucl. Instrum. Methods Phys. Res., Sect. B*, 2010, **268**, 1818-1823.
26 F. Cappella, A. d'Angelo and F. Montecchia, *Nucl. Instrum. Methods Phys. Res., Sect. A*, 2010, **618**, 168-175.
27 M. B. Smith, T. Achtzehn, H. R. Andrews, E. T. H. Clifford, P. Forget, J. Glodo, R. Hawrami, H. Ing, P. O'Dougherty, K. S. Shah, U. Shirwadkar, L. Soundara-Pandian and J. Tower, *Nucl. Instrum. Methods Phys. Res., Sect. A*, 2015, **784**, 162-167.

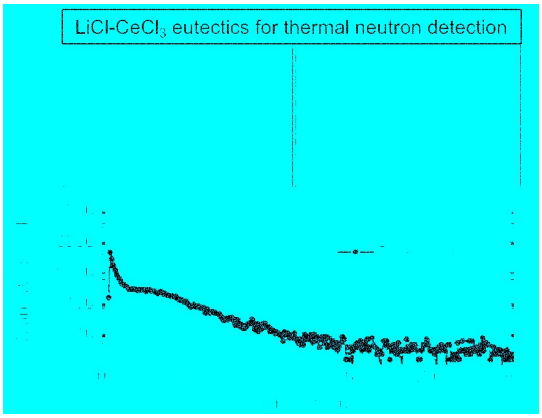

We developed novel LiCl-$CeCl_3$ eutectic scintillators that are capable of detecting thermal neutron.